

Systematic quantification of gene interactions by phenotypic array analysis

John L Hartman IV and Nicholas P Tippery

Address: Fred Hutchinson Cancer Research Center, 1100 Fairview Avenue North, Seattle, WA 98109, USA.

Correspondence: John L Hartman. E-mail: jhartman@fhcrc.org

Published: 29 June 2004

Genome Biology 2004, **5**:R49

The electronic version of this article is the complete one and can be found online at <http://genomebiology.com/2004/5/7/R49>

Received: 2 April 2004

Revised: 12 May 2004

Accepted: 19 May 2004

© 2004 Hartman and Tippery; licensee BioMed Central Ltd. This is an Open Access article: verbatim copying and redistribution of this article are permitted in all media for any purpose, provided this notice is preserved along with the article's original URL.

Abstract

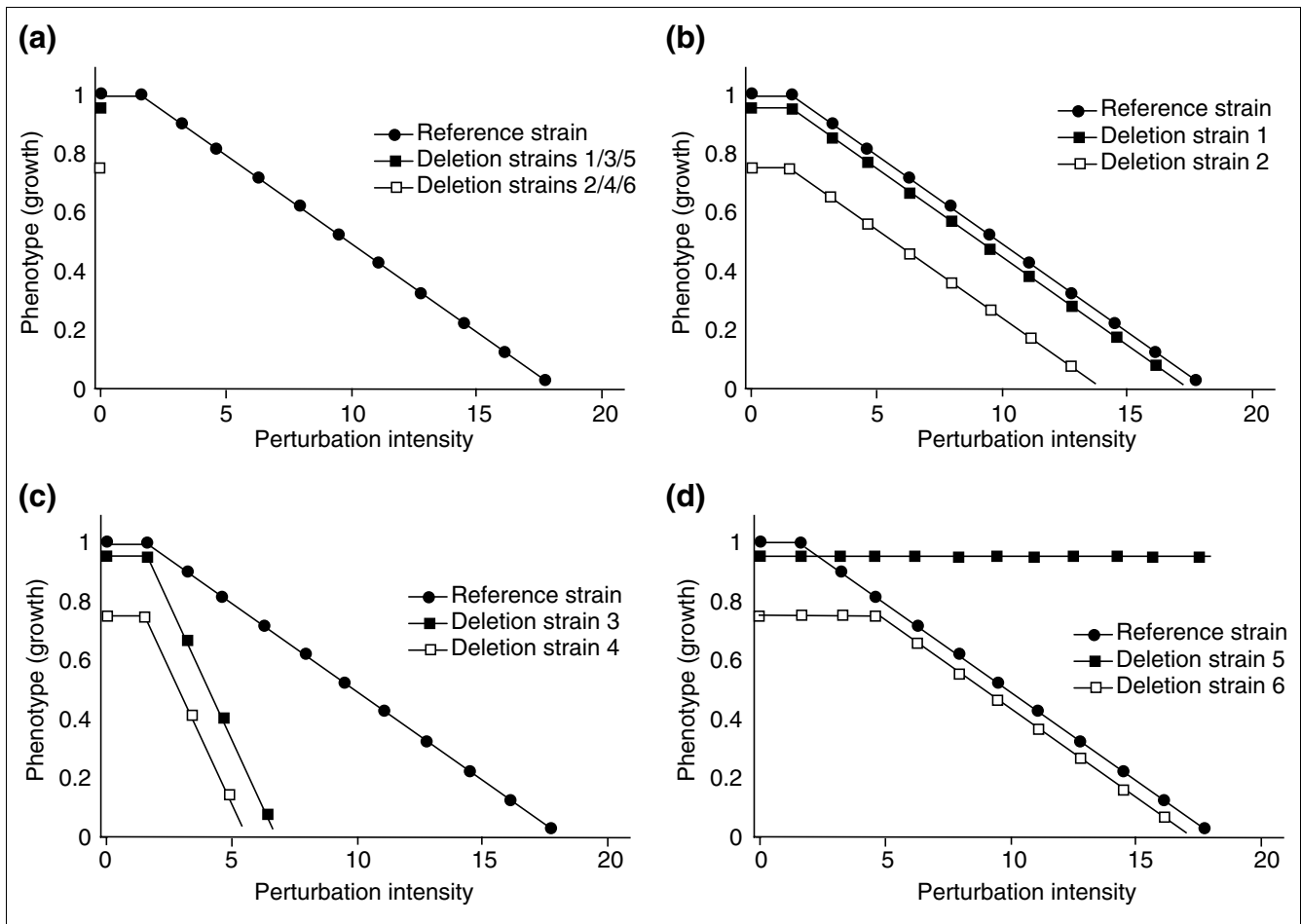
A phenotypic array method, developed for quantifying cell growth, was applied to the haploid and homozygous diploid yeast deletion strain sets. A growth index was developed to screen for non-additive interacting effects between gene deletion and induced perturbations. From a genome screen for hydroxyurea (HU) chemical-genetic interactions, 298 haploid deletion strains were selected for further analysis. The strength of interactions was quantified using a wide range of HU concentrations affecting reference strain growth. The selectivity of interaction was determined by comparison with drugs targeting other cellular processes. Bio-modules were defined as gene clusters with shared strength and selectivity of interaction profiles. The functions and connectivity of modules involved in processes such as DNA repair, protein secretion and metabolic control were inferred from their respective gene composition. The work provides an example of, and a general experimental framework for, quantitative analysis of gene interaction networks that buffer cell growth.

Background

The contributions of genes to phenotypic traits are modified by interactions with other genes and the environment, resulting in heterogeneity of monogenic disease traits and the unpredictable penetrance of complex disease [1,2]. Statistical genetic methods, used for detecting gene-phenotype associations in natural outbred populations, are not powerful enough to detect interacting effects due to the combinatorial complexity of genetic and environmental variations [3,4]. In contrast, experimental genetic methods relying on inbred genetic backgrounds and controlled environments have found phenotypic enhancement and suppression to be ubiquitous [5-7]. However, the dependence of interactions upon genetic background and environmental conditions is usually de-emphasized, resulting in a bias toward biological oversimplification [5,8,9]. The primary aim of this work is to formalize an experimental framework for global analysis of phenotype modification through quantification of gene interactions.

Genome sequencing has enabled the study of all genes in parallel, enabling systems biology and an integrated experimental understanding of all gene functions [10]. It is hoped that the outcome will be more detailed knowledge about the complex genetics of natural phenotypes, such as human diseases. This vision is partially embodied by a concept - 'genetic architecture' - referring to the full range of effects that modify genetic traits [3]. Understanding genetic architecture will require more systematic, comprehensive and quantitative knowledge about how phenotypic stability is influenced by interacting genetic and environmental variations (Figure 1). Experimentally derived principles of gene interaction, such as how gene-interaction networks function to buffer phenotypic changes against genetic and environmental perturbations, may guide hypotheses about natural phenotypic variation [5,6,11,12].

Given the respective goals and limitations of studying inbred and outbred genetic systems, molecular and population

**Figure 1**

Model for classifying interactions as additive or non-additive. The interaction of effects between gene deletion and a second perturbation is quantified by comparison between the reference strain and each deletion strain over a range of perturbation-induced effects. Six hypothetical deletion strains are depicted to illustrate the contrast between additive and non-additive interaction. **(a)** The 'phenotypic slope' of the reference strain (filled circles) defines the effect of perturbation on the reference strain. The effect of gene deletion is determined in the absence of perturbation, and typically has either no effect (strains 1, 3, and 5) (filled square) or a negative effect (strains 2, 4, and 6) (open square) on growth. **(b)** Additive gene interactions are defined by the phenotypic slope of the deletion strain being parallel to that of the reference strain, across a range of perturbations (strains 1 and 2). **(c,d)** Non-additive gene interactions can be either synergistic (c), giving a phenotypic slope of greater absolute value (strains 3 and 4), or antagonistic (d), giving a phenotypic slope of lesser absolute value (strains 5 and 6). Two types of antagonistic interactions are depicted in (d). Deletion strain 5 is absolutely antagonistic to the perturbation (for example, drug resistance due to loss of a transporter required for drug uptake), whereas deletion strain 6 is antagonistic only when the inhibitory effect of the deletion alone is greater than that of the perturbation alone (for example, drug resistance due to deletion of the gene encoding the protein target of drug inhibition).

geneticists think about gene interaction differently [4,9,13-16]. Our work defines interaction quantitatively as 'non-additive phenotypic effects resulting from combining two discrete perturbations' (Figure 1). Biologically, non-additive phenotypic interactions provide a mechanism for the accumulation of functional genetic variation in a population, because interacting alleles, subject to phenotypic selection when present in combination, may escape selection and accumulate within a population by genetic drift in the absence of the interacting partner. In contrast, additive effects reflect genetic or environmental perturbations that elicit independent cellular

responses, and thus phenotypic selection is less dependent on combinations.

Using the isogenic yeast deletion set, which provides both genetic tractability and genome wide insights, we developed a method for quantifying gene interaction globally with respect to cell growth. The phenotypic effects of experimental perturbations (for example, gene deletion and drug exposure) are measured individually and in combination for all deletion strains in parallel [17], and then quantified as additive, synergistic (greater than additive), or antagonistic (less than

additive) (Figure 1). The expression 'additive interaction' implies that phenotypic effects are expressed independently, synonymous with 'no interaction' [4,9].

Is it possible to understand gene interaction networks comprehensively and quantitatively? A simplifying principle is that biological systems appear modular (for example, pathways) [18], so that network organization may be understood by the links between sets of functionally related genes. Genes and pathways that interact with respect to phenotype are said to buffer genetic variation [5,6]. As gene mutations typically cause loss of function, the set of yeast deletion strains provides a powerful resource for investigating the genetic basis of phenotypic buffering. With the aim of conceptualizing an experimental framework for global quantitative analysis of gene interactions, this work involves development of a platform for measuring phenotypic interactions and demonstrates how quantitative analysis aids formulation of hypotheses about how cell growth is buffered against inhibitory perturbations. The analysis focuses on hydroxyurea (HU), an inhibitor of ribonucleotide reductase (RNR). RNR is a highly regulated protein complex required for deoxynucleoside triphosphate (dNTP) synthesis, DNA replication and repair, and cell proliferation [19-27], and thus plays a central role in the molecular events of genome replication and cancer.

Results

The phenotypic array: theoretical and technical considerations for high-throughput growth analysis

Growth is both a system-level readout of cellular function and a quantitative trait. There are many considerations in quantifying growth, which is a complex function of cell proliferation, cell size, and viability/life span: each is potentially affected by genetic background (that is, gene deletions) and environmental factors (for example, temperature, nutrient conditions, drugs).

The phenotypic array method is based on analysis of scanned images of 8×12 cellular arrays spotted onto agar growth medium (Figure 2). In pilot studies, the image density of spotted cultures was linearly related to the number of cells (data not shown); however, imaging sensitivity was insufficient to measure exponential growth rates directly (see part A of the figure in Additional data file 1). Thus, we used the area under the growth curve (AUGC) as a unit measure of growth, representing the overall fitness (rate and total yield) for biomass accumulation (Figure 2).

The growth index: a measure for screening non-additive gene interactions

The growth index (GI) predicts whether a deletion strain maintains growth proportional to the reference strain under a single perturbation. The equation is given in Figure 2i. It is formulated as a z-statistic, providing a standardized

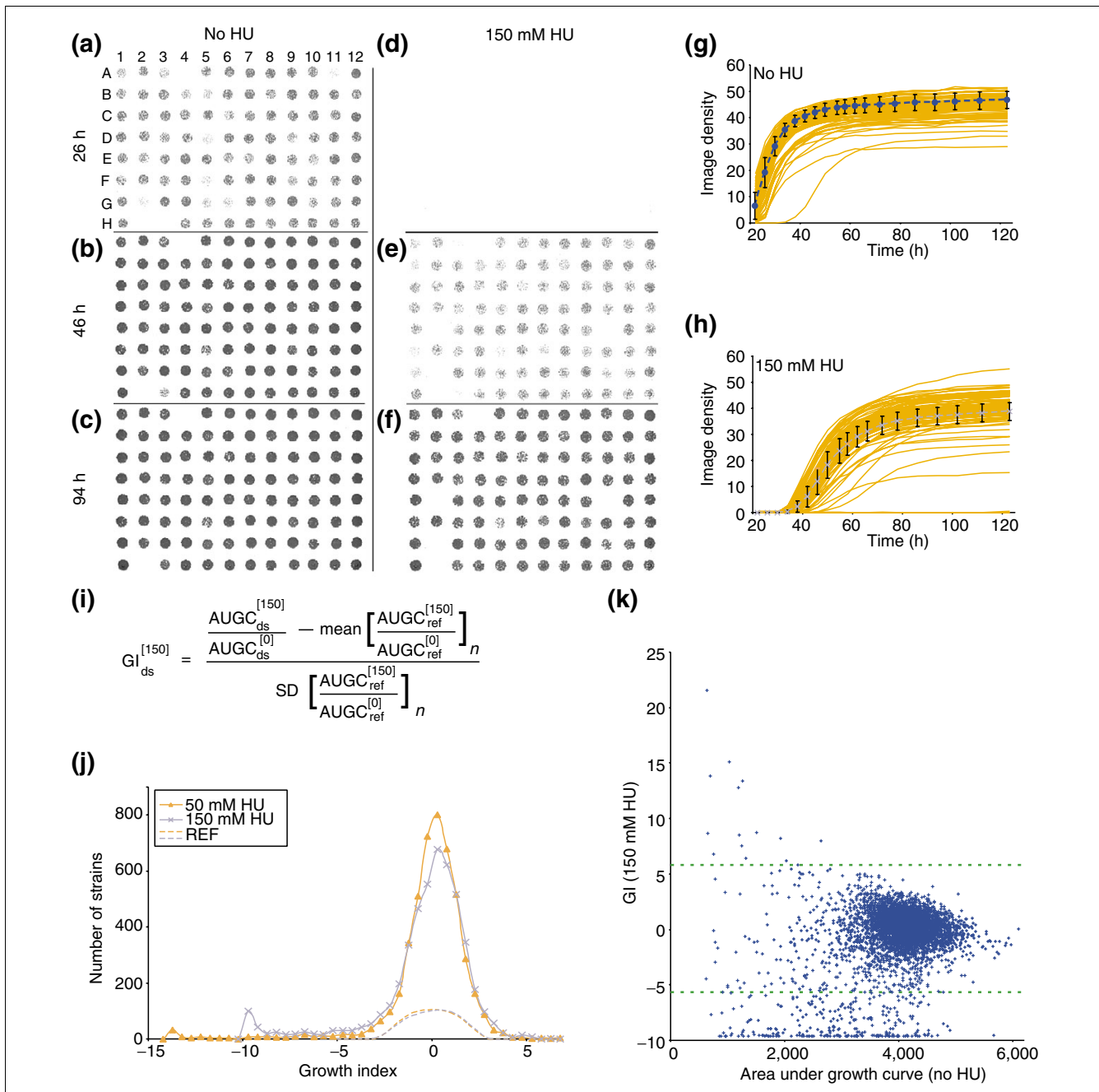
comparison of interactions. The rationale for each of the terms in the GI equation is as follows. First, the growth (AUGC) of each deletion strain under a perturbation is normalized to 'intrinsic growth' (AUGC of the same strain without perturbation) to account for effects of the deletion alone (see Figure 1, and Additional data file 2). Second, the mean and standard deviation of normalized growth for replicate cultures of the reference strain represent the effect of the perturbation alone and the experimental noise, respectively. Thus, a non-zero numerator signals a differential phenotypic response to the perturbation between the deletion strain and the reference strain, and the denominator normalizes to the experimental noise (Figure 2i).

Slow growth was found to be noisy; harsher perturbations therefore result in higher minimum GI values (Figure 2j). Also, strains with high GI values (antagonistic interactions) usually consist of intrinsically slow-growing strains having relative resistance but not better absolute growth than the reference strain (see Figure 1d, and Additional data file 2) [28]. The GI may be modified to quantify the effect of a single perturbation (that is, gene deletion or drug exposure), whereby the AUGC, with and without perturbation, is substituted for the normalized ratios (for example, see column J in Additional data file 7). The GI, as a z-statistic, is normally distributed for replicates of the reference strain, with a mean value of zero (Figure 2j, and parts A and B in Additional data file 4), and is robust with respect to times after which growth has largely subsided (linear regression of GI values from the genome-wide HU screen calculated at 94 versus 123 hours had $R^2 = 0.986$, data not shown). Reproducibility of GI measurements obtained from independent experiments is represented in Additional data file 3.

A common method for recording growth phenotypes involves comparing serial dilutions of cells spotted onto agar [29,30]. Because we use a single dilution across a range of perturbations, and the AUGC is a fairly novel unit measure for growth, we examined the behavior of the GI with respect to the perturbation strategy (cell dilution versus drug dilution) (see Additional data file 4). Drug dilution and cell dilution were well correlated with respect to GI, but only drug dilution quantitatively delineates strong phenotypic interactions: for example, when drug dilution but not cell dilution permits growth (Figure 3).

Genome-wide HU screen reveals many non-additive interactions

The GI was used to screen for phenotypic interactions between gene deletion and three concentrations of HU (0, 50 and 150 mM). GI scores, for replicates of the reference strain, were normally distributed around a mean of zero with a range of -2.41 to +2.15 (Figure 2j). The distribution for deletion strains is typically bimodal: one mode with a mean of zero, like the reference strain, and one with a minimum value corresponding to zero growth (see Figure 2j, and Additional

**Figure 2**

Overview of phenotypic array and growth index (GI). Growth is quantified by image analysis of cellular arrays and plotted against time to calculate area under the growth curve (AUGC), which is used to calculate the growth index (GI) a predictor of non-additive gene interaction. **(a-f)** Raw data from growth of a single deletion strain source plate (plate 4, see Additional data file 7) at three different times, 26 h (a,b), 46 h (b,e), and 94 h (c,f), and under two different conditions, synthetic complete medium without HU (a-c) and with 150 mM HU (d-f). Only three strains (E2, E10 and G2) were selected for further testing from this plate, having $GI < -5.8$. **(g,h)** Growth curves (red) for all 94 strains are plotted, along with the mean growth (blue dashed line) from 196 replicates of the reference strain, in (g) the absence or (h) the presence of 150 mM HU. **(i)** The GI equation is a z-statistic, where the difference between normalized growth of the deletion and mean of reference strains is the signal for non-additive interaction, and the standard deviation of the reference strain growth is the noise. [], concentration of HU (mM); ds, deletion strain; ref, reference strain; n , number of replicates; SD, standard deviation. **(j)** The distribution of GI scores for all strains (except 64 strains with unperturbed AUGC < 600, see Additional data files 2, 7) from the 50 mM (red triangles) and 150 mM (blue crosses) HU screens ($n = 4,788$, bin size = 0.5), along with the distribution of reference strain GI values (dashed lines) ($n = 192$, bin size = 1; range: $-2.41 < GI < 2.15$). REF, reference strain. **(k)** Plot of intrinsic growth (AUGC when unexposed to drugs) vs phenotypic interaction with HU (GI) is shown for all deletion strains. Dashed lines indicate the GI cutoffs used to select synergistic ($GI < -5.8$) or antagonistic ($GI > 5.8$) interactions for further testing.

data files 4, 7). 'Sensitivity' to HU has been reported for yeast deletion strains identified from screens of sensitivity to gamma irradiation or the alkylating agent, methyl methanesulfonate (MMS) [31,32]. We found 'synergism' among many (75/118) of these previously reported genes, as well as many others (see Additional data file 8). Different methods of scoring growth and gene interaction, different growth media, and different HU concentrations may account for inconsistencies. There was only one deletion strain, *kre22*, which was found in both of the above studies but not in our screen. This proved to be a false-negative result in our screen when we sequenced the deletion barcode from our presumed *kre22* deletion culture (see methods) [17,33] and found a contaminating strain. We subsequently recloned the *kre22* deletion and confirmed the synergistic interaction with HU in separate tests (data not shown).

Figure 2k depicts the relationship between effects of gene deletion alone and the interacting effects of gene deletion and treatment with 150 mM HU. On the basis of synergistic interaction, 274 strains were selected for further characterization, and 22 were selected on the basis of antagonistic interaction (Figure 2k, and see Additional data files 2, 8). Using the GI threshold of ± 5.8 , 94 strains met the GI criteria for both the 50 and 150 mM perturbations and 178 only for the harsher 150 mM HU condition. Only two interactions were scored as synergistic in the 50 mM HU screen alone. From Figure 2k note that antagonistic interactions ($GI > 5.8$) always occurred in the context of low intrinsic growth (see Figures 1d, 3d). This effect of 'alleviating' the deleterious effects of mutation was previously reported in transposon-mutagenized bacteria [28]. Strains with extremely low intrinsic growth ($AUGC < 600$ on C media) were excluded from GI analysis (see Additional data file 7) the small denominator means relatively slight absolute differences in perturbed growth have a disproportionately large effect on the GI (see Figure 2i) in this setting, and are thus less reproducible. Among these excluded strains, there were at least two strains (*gnd1* and *ism1*), which appeared growth-enhanced by the presence of HU; however, these were not studied further (see Additional data file 7).

In addition, the *rnr3* and *sml1* deletion strains were added to the HU-selected strains as negative controls in further studies, because while these two genes are known to regulate RNR activity [34-36], they have small or undetectable effects on HU sensitivity.

The interaction index: verification of Growth Index screening and measurement of interaction quantities

The purpose of the GI is to screen for interactions using single perturbations (Figures 1, 2i). To validate its utility and further quantify the strength of the interactions, the 298 strains (with GI less than -5.8 or greater than 5.8) selected from the HU screen were perturbed with a range of HU concentrations inducing a wide spectrum of growth inhibition in the reference strain (Figure 3, and Additional data file 1). 'Phenotypic

slopes' were calculated by regression analysis of AUGC, measured for each strain as a function of HU concentration (see Figures 1, 3, Materials and methods, and Additional data file 12). An 'interaction index' was formulated, essentially by substituting phenotypic slope values into the GI equation, yielding a z-statistic (see Figure 2i, Materials and methods, and Additional data file 12) where more negative, parallel, or less negative phenotypic slopes yield interaction index scores reflecting the probability of synergistic, additive or antagonistic interactions respectively (Figures 1, 3, and Additional data file 12). The reference range for the interaction index (replicate cultures of the reference strain) was -2.64 to $+2.04$, (see Additional data file 12). Using a z-score cut-off of ± 5.8 , 215 interactions were non-additive (197 were synergistic; 18 antagonistic), and 79 (27%) were additive (see Additional data file 12).

Genes with related functions had quantitatively similar interaction index scores. For example among the *RAD52* epistasis group (*MRE11-RAD50-XRS2*, *RAD51*, *52*, *54*, *55*, *57*, *59*, and *RDH54*) [37], all members showed equivalently strong synergistic interaction except for *RAD59* (Figure 3a, and Additional data file 12), and *RDH54*, which functions in meiosis and was not selected from the HU screen [38]. To confirm the weaker interaction of *rad59*, the respective homozygous diploid deletion strain was sporulated and dissected, the chromosomal deletion was confirmed by tag-sequencing (see Materials and methods), and multiple haploid segregants (of both mating types) were re-tested along with the homozygous diploid, which confirmed the phenotypic difference (data not shown). Thus, *RAD59* is unique among homologous recombination genes in being relatively dispensable in the context of HU stress [39].

The interaction index for each of the 11 vacuolar H^+ -ATPase deletion strains was also uniform (see Additional data file 12), but in contrast to homologous recombination, the phenotypic effect of losing the vacuolar H^+ -ATPase was additive with the effect of HU (Figure 3b). The functional modularity seems to be due to the structural requirement of each subunit for complex assembly [40].

Several deletion strains required for vesicular protein trafficking displayed synergistic phenotypic effects (Figure 3c, and Additional data file 12). Modularity within this set of genes was suggested by the vacuolar protein sorting (VPS) genes, with near-exclusive recovery of class C and D VPS mutants, which displayed non-additive interactions, while the *vps28* (the only 'non-class C/D' mutant) interaction was additive (see Additional data file 12). Furthermore, *chc1*, *clc1* and *end3*, involved in plasma membrane to vacuole trafficking [40], shared similar interaction index scores (see Additional data file 12), further implicating vacuolar trafficking as an important module for buffering HU stress.

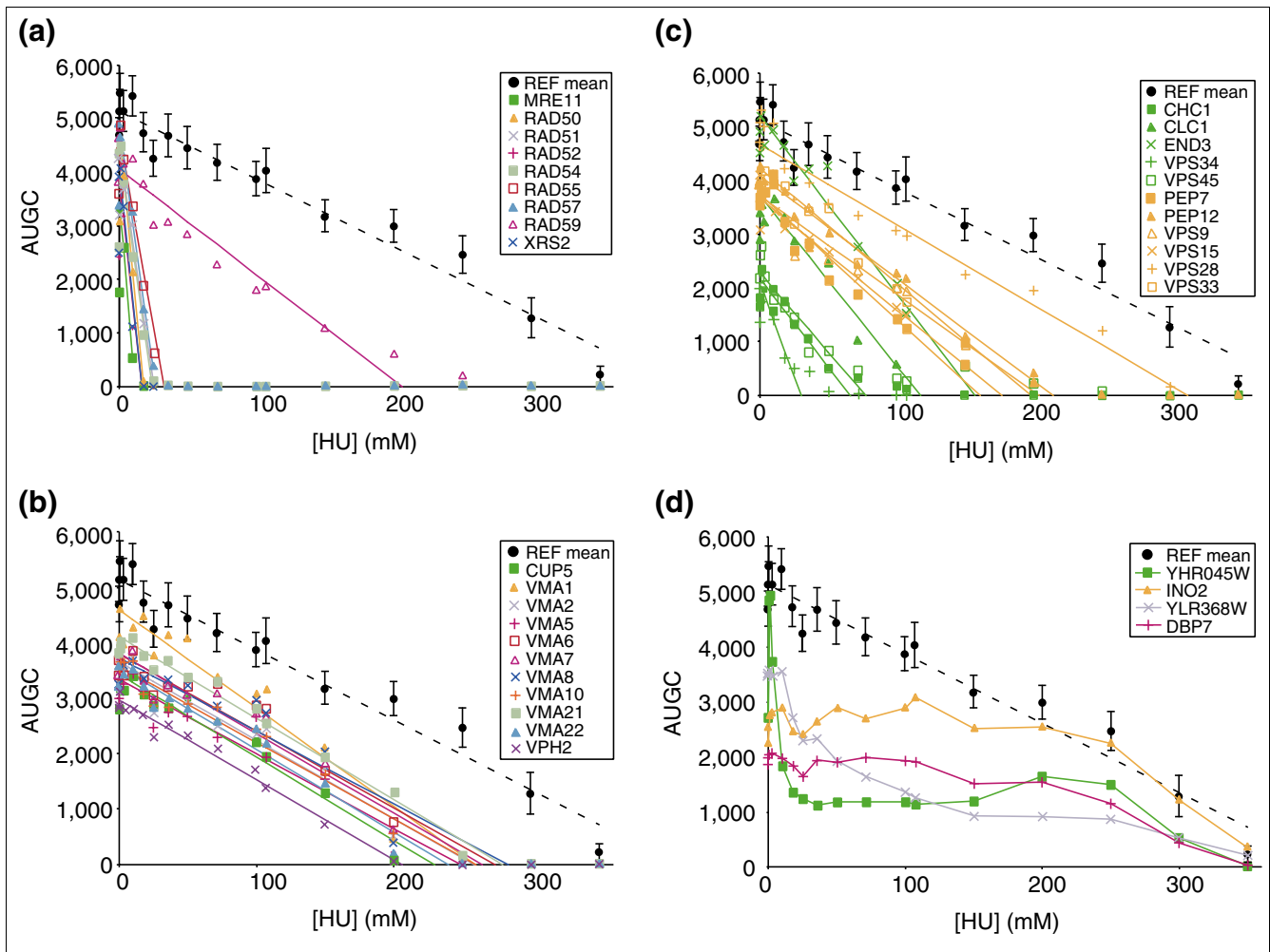


Figure 3
Modularity in buffering growth against HU inhibition is exemplified by genes with related functions having similar strength of interactions. AUGC is plotted vs HU concentration in all cases. **(a)** Genes of the RAD52 epistasis group. Note the uniformly strong synergistic interaction (see Figure 1c), with the exception of RAD59. **(b)** Genes of the vacuolar H⁺-ATPase. Note the additive interactions (see Figure 1b). **(c)** Genes involved in vacuolar trafficking. The stronger interactions are shown in green. **(d)** Assorted examples of antagonistic interactions (see text and Additional data file 12). Note that gene deletions often, in general, antagonize the HU phenotype at concentrations where the growth inhibitory effect of the deletion is greater than the inhibitory effect of HU on the reference strain (see Figure 1d) [28]. REF, reference strain BY4741 (see Materials and methods).

Table 1

Comparison of GI values between homozygous diploid and MATa haploid deletion strains

	Synergistic HU50	Antagonistic HU50	Synergistic HU150	Antagonistic HU150	Intrinsic growth < 14%
MATa haploid only	42	18	52	4	23
Homozygous diploid only	86	76	213	72	91
Both	82	4	182	4	32
Neither	4,336	4,448	4,099	4,466	4,546
Total	4,546	4,546	4,546	4,546	4,692

At 50 and 150 mM HU, threshold values (GI < -5.8 classified as synergistic or GI > 5.8 classified as antagonistic) were used to score agreement. Only deletion strains having intrinsic (unperturbed) growth greater than 14% that of the reference strain in both sets (see text) were compared. See also Additional data file 14.

Eighteen strains exhibited antagonistic interactions (Figures 1d, 3d). Phenotypic slopes were relatively nonlinear in the context of antagonistic interactions, as absolute growth of deletion strains almost never exceeded reference-strain growth for a given perturbation (Figure 3d, and Additional data file 12: note R^2 values for strains with interaction index > 3).

There were nine strains (out of 4,852) with growth index greater than 5.8 or less than -5.8 at the 50 mM concentration only (see Additional data file 8, bolded values). The interaction index (see Additional data file 12) indicated these were spurious screening results due to experimental noise, either that associated with low intrinsic growth of the deletion strain and/or that of random experimental variation.

Reproducibility of interactions between haploid and diploid deletion strains

The analysis of phenotypic slope and interaction index given above verifies whether interactions are non-additive. It does not, however, insure that the interactions are biologically explained by deletion of the targeted gene. Unintended secondary mutations may occur during knockout transformation, and/or spontaneous growth-enhancing mutations may become fixed during strain propagation. To assess these possibilities, the genome screens were replicated in the homozygous diploid deletion set [41].

The comparison is summarized in Table 1 (see also Additional data files 7, 13, 14). Generally, the effect of homozygous deletion was more detrimental than haploid deletion for both intrinsic growth and HU resistance, consistent with previous data showing haploid deletion strains less affected by ionizing radiation and other DNA-damaging perturbations [31]. From the 150 mM HU screens, there were 182 strains from both sets indicating synergistic interaction, 52 from the haploid but not the diploid set, and 213 from the diploid set only. Some deletion strain pairs could not be directly compared using the GI because either the haploid or the diploid deletion strain had inadequate intrinsic growth (less than 14% that of the reference strain) or the deletion was not represented in both sets.

In summary, the agreement between haploid and diploid screens supports the utility of the yeast deletion set and the GI for quantifying gene interactions. It appears that the haploid deletion strains are generally more fit than their homozygous diploid counterparts, whether perturbed by HU or not. It is possible that rapid accumulation of suppressor/adaptive mutations occurs on some haploid backgrounds, but given the small population size of each culture and the small number of selective generations, accumulation of suppressors seems an improbable general explanation for the increased fitness of haploid strains [42,43].

Selectivity of interactions determined with other drug perturbations

The 298 deletion strains chosen from the HU screen were perturbed with four other drugs to determine the selectivity of gene interaction. Inhibitors of biologically diverse cellular functions were used: miconazole is a specific inhibitor of Erg11p, essential for ergosterol synthesis; cycloheximide is a specific inhibitor of Rpl28p, part of the large ribosomal subunit [44]; cisplatin causes DNA intra- and inter-strand cross-links, resulting in DNA breaks; t-butyl hydroperoxide (TBHP) induces oxidative stress. Three concentrations of each agent were identified that inhibited reference strain growth equivalently to 50, 100 and 150 mM HU (see Additional data file 1), and all conditions were tested in parallel.

Selectivity for interaction with HU was high (see Additional data file 9). The correlation between GI value in response to HU and either miconazole, cycloheximide or TBHP was near zero ($R^2 < 0.04$). In contrast, correlation between cisplatin and HU was higher ($R^2 = 0.13$) (Figure 4, and Additional data file 5). The greater correlation between HU and cisplatin interactions presumably reflects overlapping pathways required for growth during perturbations to DNA replication [29,31,32].

Hierarchical clustering of quantitative interaction data highlights bio-modularity

The experimental design and data structure of the phenotypic array are analogous to global gene-expression studies. The deletion strains are analogous to DNA hybridization probes for associating measurements with genes and the GI values represent directional (negative if synergistic, or positive if antagonistic) gene interaction quantities analogous to \log_2 of mRNA hybridization ratios. Thus clustering algorithms can be used for global correlation of the direction, strength and selectivity of interaction [45]. We refer to 'bio-modules' as sets of strains within a clustered phenotypic profile, indicating modular effects of the respective genes in responding to various growth perturbations (Figures 3, 4, 5, 6, 7).

GI data for the 298 HU-selected deletion strains, under all perturbation conditions, were clustered together (Figure 4, and Additional data file 10). The perturbations clustered by drug class rather than by inhibitory effect, indicating that the interacting effects of gene deletion are globally correlated by selectivity for the cellular target of each drug. If growth effects of drug inhibition and gene deletion were mostly additive, perturbations would cluster according to the degree of growth inhibition, as drug concentrations of equivalent effect were used (see Additional data file 1). HU and cisplatin perturbations clustered together with respect to the other perturbations, but separately with respect to each other (Figures 4, 5, 6, and Additional data file 6), reflecting the related but distinguishable biology of these two perturbations. As summarized below, we used gene annotations [46-48] as a guide to understanding the biology of respective phenotypic modules.

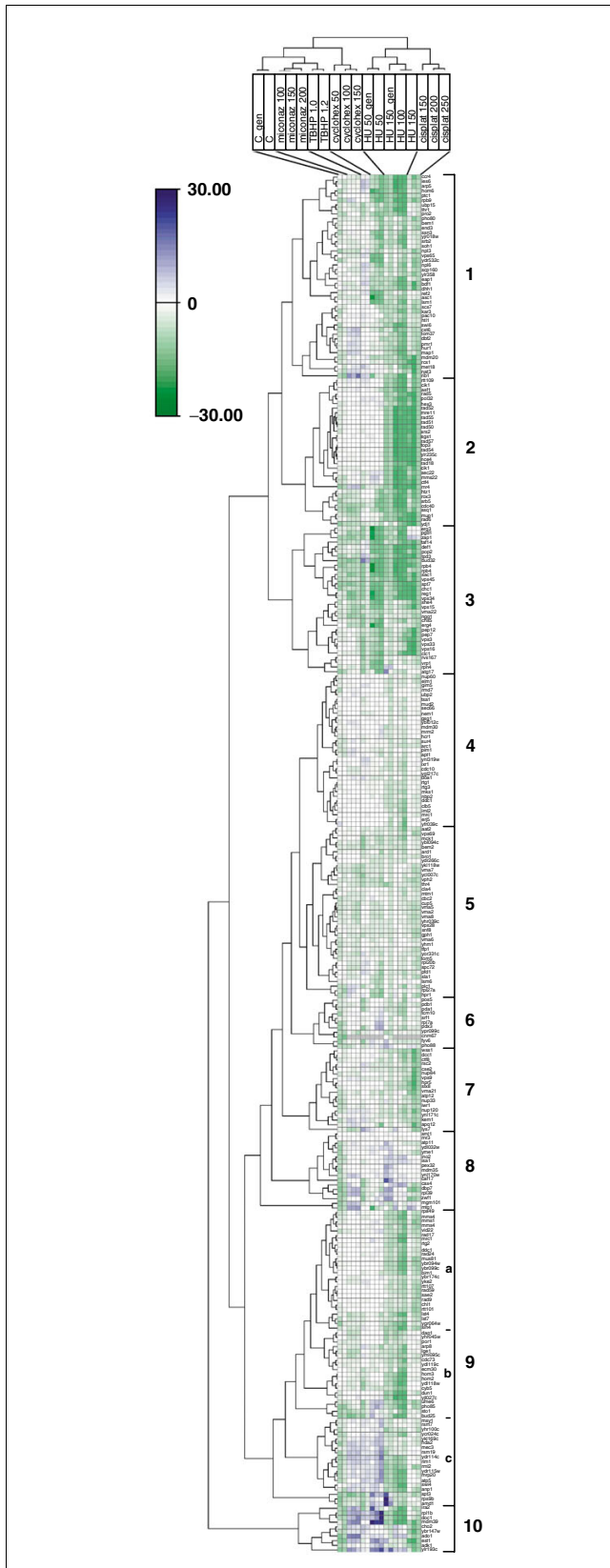


Figure 4

Figure 4

Modularity of gene interactions. The 298 HU-selected strains were perturbed with other drugs, and GI values were analyzed by hierarchical clustering. The color intensity represents the magnitude of the GI, green being negative (synergistic effect of gene deletion), but note that the range of color intensity may be different for each perturbation (see Figure 2j and Additional data file 3) because the phenotypic noise, determined for replicates of the reference strain, is measured uniquely for each perturbation (see Figure 2i). Gene clusters were given numbers (on right) for ease of referral, based subjectively on their appearance with respect to the dendrogram branches (see also Additional data file 10). GI values are reported in Additional data file 9. The first two columns (C) indicate the GI for unperturbed deletion strains (synthetic complete media, no drug). 'gen' indicates data from the original genomic screen. Otherwise, data are from a single retest of selected strains. The other columns indicate drugs used for perturbation as follows (numbers following the abbreviation indicate the concentration): miconaz, miconazole (nM); TBHP, t-butyl hydroperoxide (mM); cyclohex, cycloheximide (ng/ml); HU, hydroxyurea (mM); cisplat, cisplatin (μ M). The drug perturbations and the growth phenotypes for the reference strain under each perturbation are given in Additional data file 1. Gene names are from SGD and descriptions can be found in Additional data file 10 [47].

The strains in cluster 2 (Figure 4) indicate strong synergistic effects, selective for HU and cisplatin perturbations. This cluster is enriched for DNA repair functions (Figure 5a), including recombination pathways [49,50]. The biological basis of this module probably relates to increased requirement for repair of single-strand DNA gaps and/or DNA double-strand breaks resulting from stalled replication forks as a consequence of either dNTP pool limitation or DNA cross-links [19,20,23,51,52]. Mre11p, Rad50p, and Xrs2p, along with the products of other genes in the *RAD52* epistasis group, comprise a protein complex that repairs DNA breaks by homologous recombination. Rad51p has recombinase activity that is stimulated by Rad55p, and it is targeted to single-stranded DNA by Rad52p [37,48]. *SGS1* (Bloom's Syndrome/RecQ helicase homolog), *TOP3* (*SGS1*-interacting topoisomerase), *MUS81*, *MMS4*, and *HPR5* have been characterized for their roles in detoxifying single-strand DNA lesions (see Figure 6b) [52]. Within cluster 9a, five of six genes involved in sensing DNA damage (*RAD24*, *RAD17*, *RAD9*, *DDC1* and *MRC1*) form a module, while *MEC3* appears distinct, not interacting with cisplatin, and interacting antagonistically with other perturbations (Figure 4, cluster 9c, and Figure 6b). Only a few nucleotide-metabolism genes were identified from the HU screen. The interaction phenotypes of the strains *ado1* (adenosine kinase; converts adenosine to AMP) and *adk1* (adenylate kinase; converts AMP + ATP to ADP) were antagonistic, suggesting that the slow-growth phenotype of these strains could be due to basal substrate limitation. Thus, the growth-inhibitory effect of HU, observed at lower concentrations in the reference strain, would be masked until RNR activity becomes limiting (see Figure 1d) for dATP production. The strains *apt1* (encoding adenine phosphoribosyltransferase, which converts adenine and phosphoribosyl pyrophosphate (PRPP) to AMP) and *amd1* (AMP deaminase) indicated synergistic effects of gene deletion and HU perturbation, suggesting that these genes may

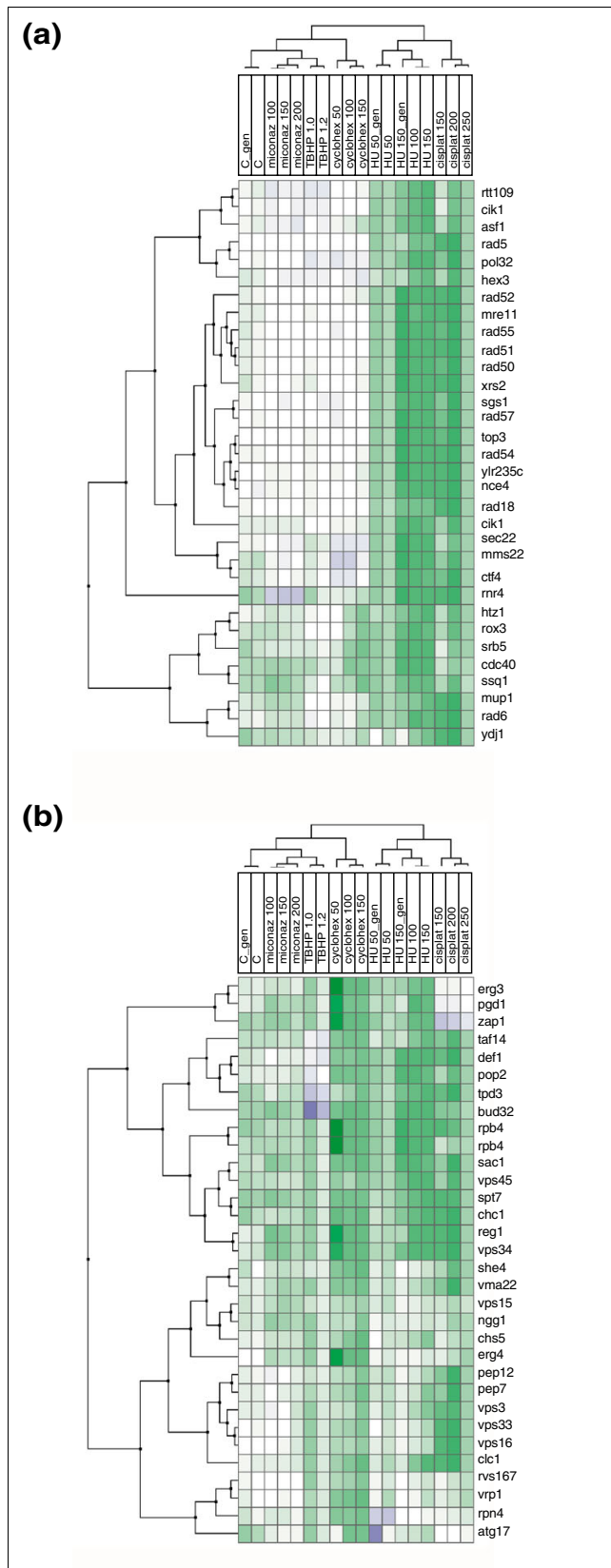


Figure 5

Figure 5

An enlarged view of clusters 2 and 3 from Figure 4. **(a)** Cluster 2 identifies a group of strains indicating strong and selective synergism between gene deletion and DNA-damaging perturbations. The set is highly enriched for DNA repair genes, and, in particular, homologous recombination genes. **(b)** Cluster 3 identifies genes required for growth under all perturbations tested, and is enriched for genes involved in vesicular trafficking, most notably vacuolar protein sorting. Gene names are from SGD and descriptions can be found in Additional data file 10 [47]. Abbreviations as in Figure 4.

have a regulatory function to compensate for growth deficiency, possibly by effecting an increase in the ADP substrate on demand. The hypothesis that ADP is the limiting substrate of RNR activity is consistent with the logic of negative feedback regulation, given that dATP is an allosteric inhibitor of RNR [22].

Threonine synthesis was another interesting module. It was the only amino-acid metabolism pathway recovered from the HU screen (see Additional data file 11). Deletion of *HOM3* and *HOM2* (homoserine is upstream of the threonine/methionine branch point) resulted in very strong and selective synergism with HU, whereas the deletion effects in downstream components (*HOM6*, *THR1*, *THR4*) were less selective (see Additional data file 5). *AAT2* (aspartate aminotransferase), which is involved in the metabolism of aspartate, the substrate of Hom3p, showed weaker synergism (see Additional data file 12).

Genes required for normal mitochondrial function (*SSQ1*, *TOM37*, *ATP5*, *RML2*) also displayed HU synergism (see Additional data file 11). Reduced RNR function causes increased respiratory deficiency, possibly owing to perturbed mitochondrial DNA replication [53]. Possibly connecting the threonine synthesis and 'mitochondrial' modules is the 'retrograde signaling' module (see Figure 7 and Discussion). *RTG1*, *RTG2*, *RTG3* and *MKS1* have been studied for their function in regulating the expression of genes of the TCA cycle [54-57] in response to mitochondrial dysfunction. Retrograde-deficient mutants are auxotrophic for aspartate, the precursor of threonine synthesis [54]. *MKS1*, which interacts with *RTG2* in retrograde signaling [56], had a similar interaction profile to the RTG genes (see part C of Additional data file 6).

The *lst4* and *lst7* (lethal with *sec13*) deletion strains, which clustered together, were phenotypically 'modular' with *rtg2* as well (Figure 4, cluster 9a). *LST4* and *LST7* (along with an essential gene, *LST8*) have been shown to regulate transport of *GAP1* (general amino acid permease) between the vacuole and plasma membrane [58]. Furthermore, *RTG2* signaling is negatively regulated by *LST8* [59]. A hypothesis emerging from these interactions is that they represent a regulatory circuit whereby metabolic flux through threonine synthesis and degradation provides glycine, which may augment purine synthesis when RNR activity is compromised (see Discussion, and Figure 7) [47,60].

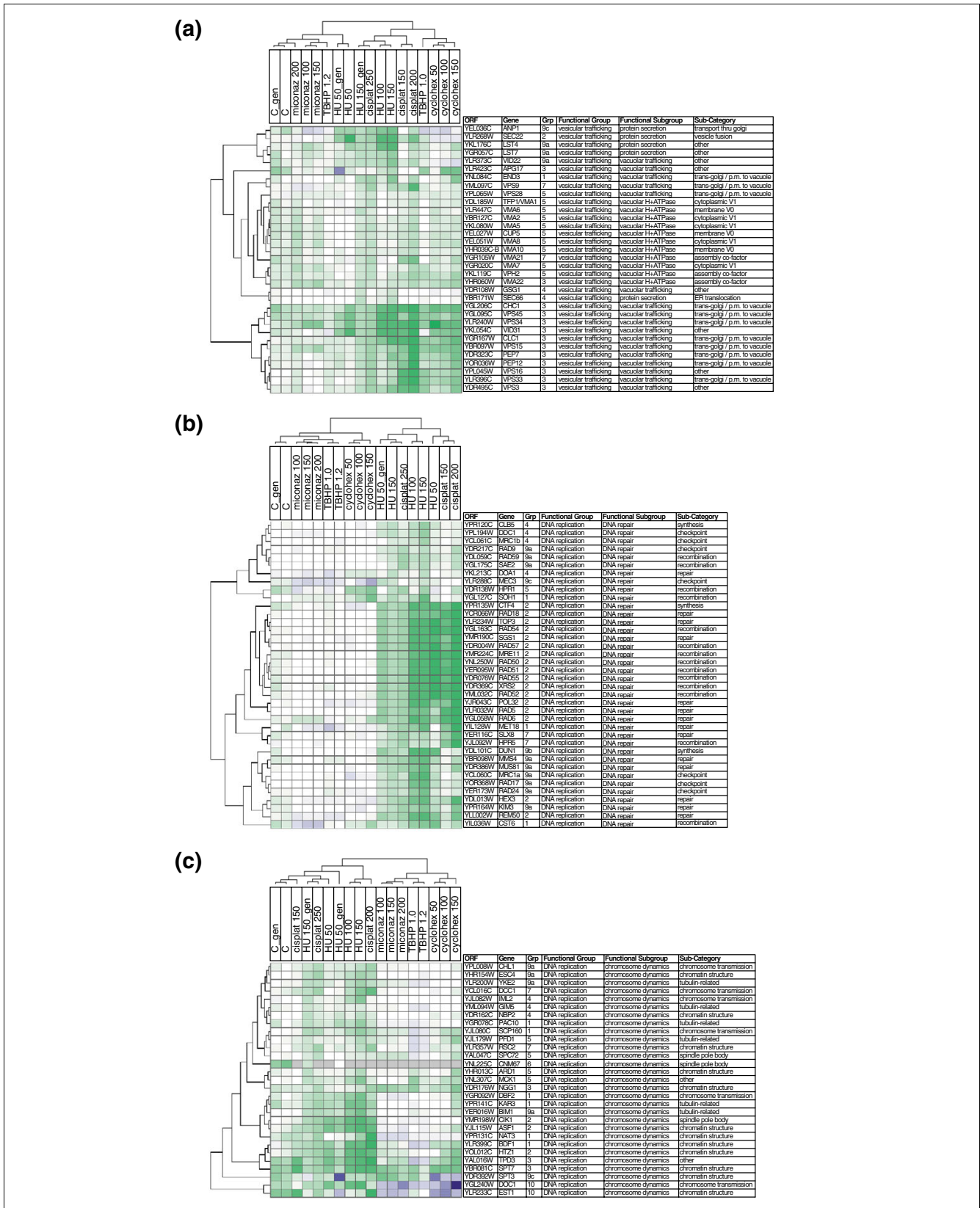


Figure 6 (see legend on next page)

Figure 6 (see previous page)

Pathway modularity, assessed by subclustering of GI data involving genes of known function for protein trafficking or DNA replication. The 298 HU-selected deletion strains were classified, based on literature annotations of their respective gene functions, into cellular pathways (see Table 2 and Additional data file 11) and sub-clustered accordingly. Color intensity corresponds to the GI (see Figure 4 for scale). Grp refers to the cluster designation from Figure 4. **(a)** Growth profiles from strains carrying deletions of vesicular trafficking genes. Note the several vacuolar protein sorting mutants (*vps* and *pep*), which share a distinctive phenotypic profile, even among other genes required for protein secretion and trafficking [30]. **(b-c)** Clustered growth profiles from strains carrying deletions in genes important for DNA replication, divided into DNA repair and chromosome dynamics (see text for further details).

A different bio-module was suggested by the broad phenotypic profile of interactions involving vesicular trafficking and vacuolar protein sorting genes [40,61], and the strong synergism with cycloheximide (Figures 4 (cluster 3), 5b). A resulting hypothesis is that *VPS* genes are generally required for growth when protein synthesis is stressed (as with ribosomal poisoning by cycloheximide), and that protein synthesis is, in fact, generally stressed when cell growth is limited (see Discussion). Support comes from previous work showing morphological class C (no vacuole) and D (defective inheritance and acidification) *vps* mutants [62] to be most defective in proliferative responses of the endoplasmic reticulum, and sensitive to a diverse array of 22 perturbing conditions [30]. Overall, only 12 of 46 *vps* mutants are in class C and D for vacuolar morphology [62]; however, nine of 10 identified in this study were class C or D (the exception being *vps28*, which was phenotypically distinct in further tests, see Figure 3c). Our findings support a previous hypothesis that increased flux through the *VPS* pathway is a compensatory response required for maintaining growth in the face of a wide range of cellular perturbations [30].

The phenotypic profiles of the *end3*, *chc1* (clathrin heavy chain) and *clc1* (clathrin light chain) deletion strains were similar to the *vps* strains (Figure 7c, and Additional data file 12), implicating their shared role in trafficking to the vacuole, via endosomes [40]. The strength of interaction for these mutants was similar to that of the *vps* mutants, further hinting at modularity in the requirement for flux through the vacuolar protein secretion pathway.

Tight phenotypic clustering was observed for strains carrying deletions of the structural subunits of the vacuolar H⁺-ATPase (*VMA1*, *VMA2*, *VMA5*, *VMA7*, *VMA8*, *VMA6*, *VMA10*, *CUP5*) (Figure 1 (cluster 5), see also Additional data file 10). Each of the subunits is essential for assembly and thus function of the complex [40]. Overall, the interactions appeared weak and non-selective, suggesting that the result of losing the vacuolar H⁺-ATPase is additive (see Figure 3b).

An example of a protein complex that does not function quantitatively as a discrete biomodule is the GIM complex (*PAC10*, *YKE2*, *PFD1*, *GIM5*, *GIM4*, *GIM3*), which is involved in protein folding and maturation of tubulin and actin [63,64]. Only four of the six subunits (*PAC10*, *YKE2*, *PFD1*, *GIM5*) were identified in the 150 mM hydroxyurea screen (see Additional data file 11). Though similarities in the interaction

profiles exist (Figure 6c), the relatively pleiotropic phenotypic effects of deleting genes of the GIM complex suggest that this complex is less modular than others in buffering growth against diverse perturbations.

Clustering sub-analysis highlights modular properties of pathways

The conclusions above about biomodules were based on enrichment of related genes within phenotypic clusters. However, genes of the same pathway may have opposite effects on pathway output, in which case phenotypic effects of gene deletion should not cluster together. For a more pathway-focused view, all genes were classified within broad categories of cellular function (gene expression, vesicular trafficking, cell polarization, DNA replication and cell metabolism) based on the literature (see Additional data file 11), and the subsets were individually clustered (Figure 6, and Additional data file 12).

The following broad conclusions drawn from the entire dataset (Figure 4) were confirmed. First, most strains deleted for known DNA replication genes interacted synergistically and selectively with the DNA synthesis inhibitors HU and cisplatin (Figure 6b,6c). Second, it appears that deletion of damage-sensing/checkpoint genes caused less synergism than loss of homologous recombination, particularly in response to cisplatin (Figure 6b). Third, genes involved in chromosome structure and movement showed quantitative effects comparable to the damage-sensing genes, but with less selectivity (Figure 6c). Fourth, strains defective in vesicular trafficking revealed interactions with many of the perturbations tested, the subset of *vps* deletions being notable for having more selective and stronger phenotypic interactions with HU and cisplatin (Figure 6a).

The pathway-oriented sub-analysis also highlighted clustering features that are less obvious when the entire dataset is analyzed (Figure 4). For example, Figure 6a recapitulates clusters 3 and 5 (from Figure 4), both composed of vesicular trafficking genes, while Figure 6b recapitulates clusters 2 and 9a, composed of genes required for DNA damage repair (Figure 6). It appears that these clusters have similar selectivity yet are quantitatively distinct as judged by strength of interaction. Overall, deletion of genes functioning in gene expression, cell polarization and cellular metabolism gave less modular phenotypic profiles, reflecting more pleiotropic interactions between deletions within these classes of genes

Table 2**Classification of all HU-selected strains, according to gene annotation [46-48]**

Functional group	Number
Gene expression	
Transcription	16
RNA processing	15
Nuclear/cytoplasmic transport	5
Translation	8
Total	44
Vesicular trafficking	
Protein secretion	5
Vacuolar trafficking	17
Vacuolar H ⁺ -ATPase	11
Total	33
DNA replication	
DNA synthesis/repair	38
Chromosome dynamics	29
Total	67
Cell polarization	18
Cell metabolism	
Cell growth	7
Mitochondria	24
Amino acid metabolism	8
Nucleotide metabolism	7
Phosphate metabolism	3
Lipid metabolism	6
Carbohydrate metabolism	6
Heavy-metal metabolism	2
Oxidative protection	3
Total	66
Unknown	67
Total	295

See Additional data file 11 for more detail.

as a function of changing cellular context (see Additional data file 12).

Discussion

Global analysis of gene interactions provides insights into the robustness of biological systems [5,6,12]. When alteration of a gene is phenotypically synergistic with a perturbation, it indicates that the unaltered gene can buffer the phenotype against that perturbation [5]. Most work on global functional

analysis of yeast phenotypes has relied upon experimental features unique to yeast, such as barcoded deletion alleles [17], on indirect measures of growth, such as PCR or microarray hybridization [17,65], or has recorded interactions qualitatively or subjectively [6,8,29,66]. To enhance opportunities for computational modeling of gene-interaction networks, we present a systematic approach for the quantification of phenotype modification.

The yeast deletion array is now an unparalleled resource for such analysis; however, the experimental method could be applied to any genetically defined cellular array (for example, with RNA interference). Furthermore, the statistical tools deployed provide a standard method of reporting gene-interaction quantities, which may help discount the effect of experimental variations due to different perturbations, different laboratories, and even different cell types. Given the essentially infinite combinatorial complexity of gene interaction and the quantitative continuum of phenotypic effects, the need for high-throughput and quantitative phenotyping is perhaps superseded only by the need for statistically comparable data that can be easily stored, shared, mined and integrated with other genomic data [67,68].

The phenotypic array method presented here easily accommodates parallel analysis of around 24,000 independent cultures per experiment. We used AUGC as a growth measure, incorporating rate and final yield into a single quantity (see Figure 2); the analysis could, however, be modified to examine interactions with respect to other parameters of growth. The GI sensitively and specifically screens for non-additive effects (see Additional data files 8, 12). Phenotypic slopes are used to derive an Interaction Index, which precisely quantifies interactions, thus confirming or refuting screening results (see Figures 1, 3, and Additional data file 12). Clustering of GI data was useful for identifying biomodules, as were gene annotations for interpreting their relatedness (see Figures 4, 5, 6, 7).

The experimentally derived topology of gene interactions is complex [6,12,29]. What is the full complement of genes required to buffer a particular perturbation, and what is the relative importance of each gene? Conversely, what is the full range of phenotypic effects that a single genetic or environmental perturbation can induce? How do the properties of gene interaction networks change as a function of time and intensity of perturbation? The complex nature of these questions calls for quantitative answers [1-5,8,9].

For experimentally deriving gene-interaction networks, what is the appropriate balance between qualitative breadth and quantitative depth of data acquisition and analysis? Anecdotal comparison of this work to that of Parsons *et al.* [29] suggests that this is an important consideration. Parsons *et al.* [29] analyzed a 69 (12 chemical-genetic and 57 gene-gene) × 5,000 (number of deletion strains) array of interactions

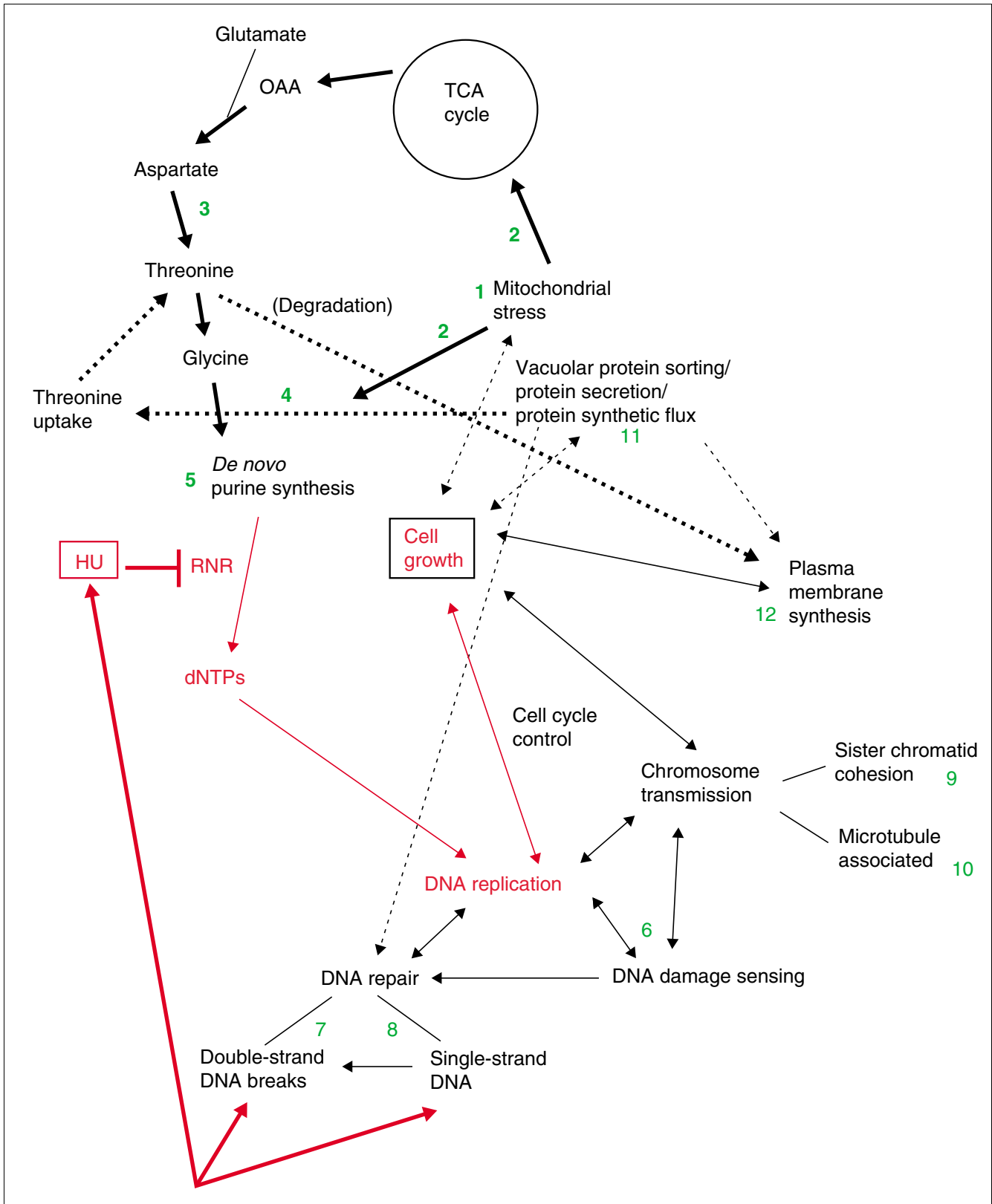


Figure 7 (see legend on next page)

comment
reviews
reports
deposited research
refereed research
interactions
information

Figure 7 (see previous page)

A speculative model for buffering against perturbation of deoxynucleoside triphosphate (dNTP) synthesis, based on interconnected genetic modules found to interact with HU. The growth inhibitory effects of HU are shown in red. Modules - sets of related genes with similar selectivity and/or strength of interactions - are indicated by green numbers (see below). Connections between modules are based on the literature about the respective genes (see Results and Discussion sections). The proposed metabolic regulation of *de novo* dNTP synthesis is indicated by bold module connections, based on recent discovery of a 'high-flux backbone' in *E. coli* [60]. Dashed lines represent related, but more speculative connections. Interaction index values, measuring the strength of interaction for all genes listed below are given in Additional data files 11, 12. Selectivity can be visualized in Figures 4-6 and Additional data file 6. 1, Mitochondrial function, *SSQ1*, *ATP5*, *TOM37*, *RML2*; 2, retrograde signaling, *RTG1*, *RTG2*, *RTG3*, *MKS1*; 3, threonine synthesis, *AAT2*, *HOM3*, *HOM2*, *HOM6*, *THR1*, *THR4*; 4, permease trafficking, *LST4*, *LST7*; 5, adenosine metabolism, *ADO1*, *ADK1*, *APT1*; 6, cell-cycle checkpoint, *MRC1*, *RAD24*, *RAD17*, *DDC1*, *RAD9*; 7, homologous recombination *MRE11*, *RAD52*, *XRS2*, *RAD50*, *RAD51*, *RAD54*, *RAD55*, *RAD57*; 8, single-strand DNA repair *TOP3*, *SGS1*, *MUS81*, *MMS4*, *HPR5*; (9) sister chromatic cohesion, *CTF4*, *CTF8*, *DCCI*; 10, microtubule associated, *PAC10*, *YKE2*, *BIMI*, *KAR3*, *CIK1*; 11, protein secretion *VPS15*, *VPS33*, *VPS34*, *VPS45*, *VPS9*, *VPS3*, *VPS16*, *PEP7*, *PEP12*, *CHC1*, *CLC1*, *END3*, *VID22*, *VID31/DEF1*; 12, membrane biosynthesis, *ERG3*, *SCS7*.

compared to our analysis of a 1 (HU) × 5,000 array plus a 5 (number of other drugs) × 300 (number of strains selected from genome-wide screen) array. Thus, qualitatively, the Parsons data represents an approximately 50-fold increase in qualitative gene-interaction data. On the other hand, our analysis of HU entailed a genomic screen at three concentrations of HU (0, 50 and 150), and then further testing of 300 selected strains on 10 different HU concentrations and three different concentrations of the other four drugs, so our study represents about a fivefold increase in 'quantitative' data. Regarding gene-interaction networks and modularity, related but different observations and interpretations emerged.

First, both studies identified the vacuolar H⁺-ATPase as a functional module. While Parsons *et al.* [29] implicated this function in multidrug resistance, our data suggest such effects are additive with HU (Figures 1, 3) [4,9,28]. Further data from Parsons *et al.* [29] indicate that the vacuolar H⁺-ATPase interacts more strongly with cyclosporin, FK506 and tunicamycin than with HU, but more weakly with camptothecin, benomyl, fluconazole and cycloheximide, suggesting that quantitative analysis of perturbations other than HU might reveal non-additive interactions between the vacuolar H⁺-ATPase mutants and these other perturbations (assuming perturbations of equivalent strength were used in the analysis of Parsons *et al.* [29]).

Second, Parsons *et al.* [29] concluded from *ERG2*, *ERG3*, *ERG4* and *ERG6* interactions that ergosterol synthesis affects multidrug resistance. Our work suggests that *ERG3* is distinct from the other ergosterol genes in the context of HU, showing much stronger synergism as well as selectivity for interaction with HU compared to cisplatin (see Figure 5, and Additional data files 7, 12). The *erg* deletion strain interaction phenotypes seemed more pleiotropic than modular in our work, varying according to the gene deleted and the particular perturbation [69].

Third, from our work, vacuolar protein sorting (VPS) buffers growth against multiple inhibitory perturbations (see Figures 3c, 5a, and Additional data file 11) [29]. Of the 10 *vps* strains (*vps3*, *vps9*, *vps15*, *vps16*, *vps28*, *vps33*, *vps34*, *vps45*, *pep7*,

and *pep12*) we found, nine are related functionally by their effects on vacuolar morphology and predicted requirement for protein synthetic flux [30,62], suggesting modularity within this class of more than 40 genes. In addition, we identified synergistic interactions between HU and 'endosome-to-vacuole trafficking' (*chc1*, *clc1*, *end3* deletion strains), perhaps also required for protein secretion flux [30]. Parsons *et al.* [29] also reported chemical-genetic interactions involving several vacuolar protein sorting deletion strains, but not with HU or camptothecin (see Figure 5 and discussion below). Furthermore, only *VPS16* was overlapping with our set in the actual VPS genes proposed by Parsons *et al.* [29] (*VPS16*, *VPS25*, *VPS36*, *VPS67*, *VAM7*, *VAM6*, *STP22*, *SNF7*, *DID4*, *IES6*) to be involved in multidrug resistance [29]. We did find *IES6* to interact strongly, but did not classify it as a VPS gene.

Fourth, the GIM complex (prefoldin actin/tubulin chaperone) (*GIM3*, *GIM4*, *GIM5*, *PFD1*, *YKE2*, *PAC10*) provides another example of contrast between quantitative and qualitative data [64]. Each study found multiple subunits to interact; however, Parsons *et al.* [29] found interactions to be benomyl-specific, while we found *PAC10* and *YKE2* to interact with HU and cisplatin (see Additional data files 6 (part C), 9). *GIM5* and *PFD1* were recovered from our screen, but were weaker interactions in confirmatory tests (see Additional data file 12). Thus our data indicate that there are more pleiotropic interactions than do the data of Parsons *et al.* [29], possibly suggesting differential requirements for each gene in the maturation of actin and/or tubulin structural proteins [64] and probably involvement of the GIM complex in buffering cell growth against a variety of inhibitory perturbations.

Fifth, both studies found homologous recombination and DNA-damage checkpoint signaling to be modular (Figures 5, 6) [29]. Our quantitative data permit the further conclusion that homologous recombination interacts much more strongly with HU, on the basis of comparison of the interaction index of the recombination group (*RAD50* (-265), *RAD51* (-171), *RAD54* (-178), *RAD55* (-138), *RAD57* (-179), *MRE11* (-304), and *XRS2* (-242)) with those of the checkpoint group (*MRC1* (-14), *RAD24* (-19), *RAD17* (-21), *RAD9* (-7), and *DDC1* (-30)) (see Additional data file 12). It may be that

functional redundancy among the checkpoint genes partially compensates for loss of these genes in response to HU, while it appears there is no such redundancy (except for *RAD59* (-7)) among homologous recombination genes. In this regard it was interesting that partial deletion of *MRC1* (YCL060c (-42)) interacted more strongly than complete deletion (YCL061c (-14)), suggesting a dominant-negative effect of the partial gene (see Additional data file 11).

Sixth, the respective studies found overlapping sets of genes required to tolerate HU and camptothecin [29], or HU and cisplatin (Figure 4). By using a continuous scale for quantifying interactions, we are able to distinguish relative strength and specificity of interaction (Figure 4, clusters 7 and 9b, and see Additional data file 4), which should enhance capabilities for computational modeling of gene interaction networks. The Parsons analysis [29] used a binary scale of interaction for cluster analysis, so did not make quantitative distinctions. However, Parsons *et al.* [29] included a wealth of qualitative interaction data, allowing comparison between chemical-genetic and gene-gene interaction clusters.

Seventh, there is a set of possibly interconnected modules from our dataset, which was essentially absent from Parsons *et al.* [29] We found all genes of threonine synthesis (*AAT2*, *HOM3*, *HOM2*, *HOM6*, *THR1*, *THR4*), several mitochondrial genes (*ATP5*, *RML2*, *TOM37*, *SSQ1*), genes involved in tricarboxylic acid (TCA) cycle regulation via retrograde signaling (*RTG1*, *RTG2*, *RTG3*, *MKS1*), and genes involved in amino-acid permease trafficking (*LST4*, *LST7*). A model connecting these modules is presented in Figure 7 and discussed below.

Understanding quantitative differences adds another dimension to interpreting the biological significance of gene interaction. Considering the cell as a highly interconnected and buffered genetic system, whenever a gene alteration occurs which predisposes a cell to cancer, for example, it also reduces the same cell's resistance to perturbations that the altered gene normally buffers against. In this example, the strength and specificity of synergism between gene loss and drug perturbation essentially determines therapeutic efficacy and toxicity. This principle of gene interaction has been proposed for drug discovery [70].

What is the biological basis for the interaction between vacuolar trafficking and DNA replication/repair? A possible clue comes from work on *VID31/DEF1*, initially identified by its requirement for targeting fructose biphosphatase (FBPase) to the vacuole for degradation upon exposure to glucose ([71] and Randy Brown, personal communication), but recently renamed *DEF1* on the basis of its association with *RAD26* and its suspected role in coordinating transcription-coupled repair of DNA damage and ubiquitin-mediated degradation of RNA polymerase II [72]. Our work shows that *VID31* deletion interacts synergistically with a broad range of perturbations, but like other vacuolar-trafficking deletion strains has

relative specificity for HU and cisplatin (Figure 6a). Recent work shows that FBPase is degraded via both the ubiquitin-proteasome-dependent cytosolic route and the vacuolar route [73], and that some genes are common to both pathways [73,74]. Thus, *VID31/DEF1* appears to have multiple functions, and further investigation of the gene interactions in this module may shed new light on the potential links between vacuolar and ubiquitin-mediated degradation pathways as well as the organization of these pathways in coordinating transcriptional control, protein degradation and DNA repair.

How might threonine synthesis buffer cell growth against the effects of HU? Almaas *et al.* [60] used flux balance analysis [75] to discover that overall metabolic activity is dominated by a small number of reactions, forming a high-flux backbone, over which metabolism is reprogrammed to optimize growth as nutrient conditions change. Threonine synthesis was found to be a major connection on this backbone, which linked respiration and the TCA cycle (which produces the threonine substrate aspartate) to purine metabolism (via catabolism to glycine with formation of one-carbon reducing equivalents) and membrane lipid synthesis. Our data support the existence of a high-flux backbone in eukaryotes (see Figure 7 and discussion above).

We propose the following speculative working hypothesis. The effect of reducing cellular nucleotide causes mitochondrial stress, either by perturbing mitochondrial replication or by other, undefined, means [21]. Retrograde signaling through *RTG1*, *RTG2*, *RTG3* and *MKS1* then acts to transcriptionally upregulate the TCA cycle [54,55], providing increased aspartate for threonine synthesis along the pathway of HU-interacting genes *AAT2*, *HOM3*, *HOM2*, *HOM6*, *THR1* and *THR4*. Threonine is then catabolized to glycine which, along a high-flux backbone [60], is used to increase purine synthesis and thus augment dNTP production by RNR. To utilize external sources of threonine for the same purpose, *LST4* and *LST7* regulate amino-acid uptake ([58] and Figure 7). Finally, *RTG2*, through its interaction with *LST8* (an essential gene that functions with *LST4* and *LST7*) [59], coordinates retrograde signaling and permease transport in regulating threonine catabolic flux, which we propose contributes to buffering of dNTP pools (Figure 7).

Conclusions

Unraveling biological complexity and understanding cells as systems will ultimately depend on the transition from identifying modules to understanding protocols [76]. This study provides a scalable methodology for identifying genetic modules, defined by their correlated strength and selectivity of phenotype modification. The work shows that modular networks of gene interaction can be deduced from quantitative phenotypic interaction data, using even a limited number of perturbations. We have presented an experimental design that is conceptually adaptable for analysis of other interaction

networks, using other perturbations. The formal methods of quantifying interactions incorporate time and perturbation intensity, providing continuous measures of interaction. Our hope is to facilitate the compilation of data, from investigators studying different areas of biology and different cell types, which is suitable for computational modeling of global gene interaction and phenotype modification. Specifically, the GI and interaction index should be applicable to quantifying the effects of systematic perturbations to other genetically defined cellular arrays, providing a resource for understanding the complexity of phenotypic modification [5,8,68,77].

Materials and methods

Strains, media, reagents and equipment

The MATa haploid deletion set was from Research Genetics (Huntsville, AL), release date 1/23/01. The reference strain, BY4741, is MATa, containing auxotrophic deletions of *his3 leu2 met17 ura3* [41]. YM-1 liquid media was used for pre-growth of the yeast deletion set in 96-well plates and Hartwell synthetic complete agar medium was used for the growth arrays [78]. HU, miconazole, cisplatin, TBHP, and cycloheximide came from Sigma. The Beckman Multimek 96, an automated 96-channel pipettor was used to inoculate, dilute and spot cultures. An Epson Expression 1640 XL scanner with A3 transparency unit was used to collect transmitted light images. For deletion strain confirmations, deletion cassettes were PCR-amplified, using the *uptag1/downtag1* primer pair [41]. PCR products were purified using the Qiagen PCR purification kit, and DNA sequencing was performed (dye terminator method) using KanB1 and KanC3 primers to identify the unique molecular barcodes [41].

Phenotypic array data collection

All strains were inoculated (1:100) from thawed, glycerol stocks into new 96-well plates containing fresh YM-1 media + 2% glucose using the Multimek 96, and pre-grown at 30°C for 36-48 h. For spotting, pre-grown cultures were resuspended by orbital shaking before diluting 1:3025 (serial 55-fold dilutions) into water using the Multimek 96. Four microliters of the 1:3,025 diluted cultures were spotted (manually, using the Multimek) to synthetic complete agar medium containing 2% glucose, 2% agar, with or without perturbing agent (poured in omni-trays, Nunc). Agar plates were typically poured at least one day before use and 'dried' (incubated with the top off) for 30-60 min at 37°C before spotting cultures. Dilution of 1:3,025 yields approximately 250-500 cells per 4 µl with the reference strain, limiting the effect of growth measurement noise due to uneven initial distribution of cells, while increasing the number of generation times for detecting growth differences (data not shown). Multiple replicates of the reference strain were used to define experimental noise due to intra- and inter-experimental variations such as dilution, suspension, and spotting of cultures. The plates were scanned at designated times (see Image analysis).

Image analysis and hierarchical clustering

Image analysis was performed on a Macintosh computer using the public-domain NIH Image program version 1.62, available on the Internet. Images were saved as 140 dpi black and white TIFF files. Up to 10 agar plates were included in a single scanned image. Scans were 'sliced' and 'stacked' to facilitate viewing and sorting data from each plate as needed for analysis. The images were then trimmed and modified to adjust for shadows, bubbles, and/or other artifacts containing pixels above the background intensity of agar. Each array (96 cultures) image contains a 600 × 400 pixel area, thus each culture in the 12 × 8 array is contained in a 50 × 50 pixel square. The average image density for each pixel of a culture, bounded by its square, is calculated using a 256-gray scale (0 = white), where values less than 90 are considered background and set to zero. The maximum pixel value within a 5-day reference strain culture spot was approximately 220; thus, maximum culture yield does not saturate the 256 gray-scale. Growth curves were created for each strain by plotting image density vs time. The TrapZ function of MATLAB version 6 was used to calculate AUGC values for each growth curve, which were in turn used to calculate the GI. Microsoft Excel was used to manipulate and analyze data further. For hierarchical clustering of GI data, we used J-Express version 2.1 (with Euclidean distance measure and complete linkage) [79].

Phenotypic slope and interaction index calculations

Phenotypic slope was determined by linear regression of AUGC vs HU concentration (mM) (see Figure 3 and Additional data file 12). For regression analysis, the first AUGC value less than 600 was the final value included; R² was greater than 0.95 (see Additional data file 12) for most strains. The interaction index was calculated like the GI (Figure 2i), substituting the corresponding phenotypic slope for each growth ratio (see Additional data file 12).

Gene classification

The gene classification was done subjectively, with reliance on the *Saccharomyces* Genome Database [47], Yeast Proteome Database [48], The Molecular and Cellular Biology of the Yeast *Saccharomyces* [46], and literature references found therein, for gene annotations.

Additional data files

The following additional data files are included with the online version of this article: figures showing determination of three concentrations of four different perturbing agents with growth inhibition equivalent to that of 50, 100, and 150 mM HU (Additional data file 1); intrinsic growth of all deletion strains and example growth curves for synergistic and antagonistic interactions (Additional data file 2); reproducibility of GI values from independent experiments (Additional data file 3); a comparison between drug dilution and cell dilution with respect to the GI (Additional data file 4); correlation

of GI values resulting from perturbation with HU and different drug inhibitors (Additional data file 5); clustering sub-analysis (based on gene classifications) of GI data from HU-interacting deletion strains, under growth inhibition with other drugs (Additional data file 6); tables showing AUGC and GI data from the genome wide screen for HU interactions (Additional data file 7); comparison of HU interactions found in different genome-wide screens (Additional data file 8); AUGC and GI data from the retest of HU-interacting strains for growth on HU, cisplatin, miconazole, cycloheximide, and t-butyl hydrogen peroxide (Additional data file 9); identity and annotation of genes depicted in Figure 4 (Additional data file 10); detailed classification of HU-selected strains (Additional data file 11); interaction index values for all HU-selected deletion strains (Additional data file 12); AUGC and GI data from the genome wide HU screen in the homozygous diploid deletion set (Additional data file 13); a comparison of the MATa haploid and homozygous diploid HU 150 screens (Additional data file 14). Legends to the figures and tables are contained in Additional data file 15.

Acknowledgements

We thank Xie L. Xu and Lue Ping Zhao for suggesting the use of AUGC and for help with the GI formulation, and David and Jacob Appelbaum for assistance with hierarchical clustering. We thank Lee Hartwell, Maynard Olson, Suzanne Rutherford, Dan Gottschling, Steve Tapscott, Jerry Radich, Leonid Kruglyak and members of their labs for helpful discussions, and Randy Brown for discussions about unpublished data (VID31). This work was supported by a grant awarded to Leland Hartwell from the National Institutes of Health, GM 17709, and by grants to J.H. from the Howard Hughes Medical Institute (Physician-Scientist Postdoctoral Fellowship) and from the NIH-NCI, CA 90637.

References

- Badano JL, Katsanis N: **Beyond Mendel: an evolving view of human genetic disease transmission.** *Nat Rev Genet* 2002, **3**:779-789.
- Moore JH: **The ubiquitous nature of epistasis in determining susceptibility to common human diseases.** *Hum Hered* 2003, **56**:73-82.
- Mackay TF: **The genetic architecture of quantitative traits.** *Annu Rev Genet* 2001, **35**:303-339.
- Barton NH, Keightley PD: **Understanding quantitative genetic variation.** *Nat Rev Genet* 2002, **3**:11-21.
- Hartman JL, Garvik B, Hartwell L: **Principles for the buffering of genetic variation.** *Science* 2001, **291**:1001-1004.
- Tong AH, Lesage G, Bader GD, Ding H, Xu H, Xin X, Young J, Berriz GF, Brost RL, Chang M, et al.: **Global mapping of the yeast genetic interaction network.** *Science* 2004, **303**:808-813.
- St Johnston D: **The art and design of genetic screens: *Drosophila melanogaster*.** *Nat Rev Genet* 2002, **3**:176-188.
- Lazebnik Y: **Can a biologist fix a radio? Or, what I learned while studying apoptosis.** *Cancer Cell* 2002, **2**:179-182.
- Phillips PC: **The language of gene interaction.** *Genetics* 1998, **149**:1167-1171.
- Ideker T, Galitski T, Hood L: **A new approach to decoding life: systems biology.** *Annu Rev Genomics Hum Genet* 2001, **2**:343-372.
- Rutherford SL: **From genotype to phenotype: buffering mechanisms and the storage of genetic information.** *BioEssays* 2000, **22**:1095-1105.
- Hartwell L: **Genetics. Robust interactions.** *Science* 2004, **303**:774-775.
- Avery L, Wasserman S: **Ordering gene function: the interpretation of epistasis in regulatory hierarchies.** *Trends Genet* 1992, **8**:312-316.
- Zeyl C: **Budding yeast as a model organism for population genetics.** *Yeast* 2000, **16**:773-784.
- Cordell HJ: **Epistasis: what it means, what it doesn't mean, and statistical methods to detect it in humans.** *Hum Mol Genet* 2002, **11**:2463-2468.
- Wagner GP, Laubichler MD, Bagheri-Chaichian H: **Genetic measurement of theory of epistatic effects.** *Genetica* 1998, **102-103**:569-580.
- Giaever G, Chu AM, Ni L, Connelly C, Riles L, Veronneau S, Dow S, Lucau-Danila A, Anderson K, Andre B, et al.: **Functional profiling of the *Saccharomyces cerevisiae* genome.** *Nature* 2002, **418**:387-391.
- Hartwell LH, Hopfield JJ, Leibler S, Murray AW: **From molecular to modular cell biology.** *Nature* 1999, **402**:C47-C52.
- Vilenchik MM, Knudson AG: **Endogenous DNA double-strand breaks: production, fidelity of repair, and induction of cancer.** *Proc Natl Acad Sci USA* 2003, **100**:12871-12876.
- Chabner B, Ryan DP, Paz-Ares L, Garcia-Carbonero R, Calabresi P: **Antineoplastic Agents.** In: *Goodman & Gilman's The Pharmacological Basis of Therapeutics* 10th edition. Edited by: Hardman JG, Limberd LE, Gilman AG. New York: McGraw-Hill; 2001:1381-1459.
- Koc A, Wheeler LJ, Mathews CK, Merrill GF: **Hydroxyurea arrests DNA replication by a mechanism that preserves basal dNTP pools.** *J Biol Chem* 2004, **279**:223-230.
- Jordan A, Reichard P: **Ribonucleotide reductases.** *Annu Rev Biochem* 1998, **67**:71-98.
- Kunz BA, Kohalmi SE, Kunkel TA, Mathews CK, McIntosh EM, Reidy JA: **International Commission for Protection Against Environmental Mutagens and Carcinogens. Deoxyribonucleoside triphosphate levels: a critical factor in the maintenance of genetic stability.** *Mutat Res* 1994, **318**:1-64.
- Desany BA, Alcasabas AA, Bachant JB, Elledge SJ: **Recovery from DNA replicational stress is the essential function of the S-phase checkpoint pathway.** *Genes Dev* 1998, **12**:2956-2970.
- Zhao X, Chabes A, Domkin V, Thelander L, Rothstein R: **The ribonucleotide reductase inhibitor Sml1 is a new target of the Mec1/Rad53 kinase cascade during growth and in response to DNA damage.** *EMBO J* 2001, **20**:3544-3553.
- Tanaka H, Arakawa H, Yamaguchi T, Shiraiishi K, Fukuda S, Matsui K, Takei Y, Nakamura Y: **A ribonucleotide reductase gene involved in a p53-dependent cell-cycle checkpoint for DNA damage.** *Nature* 2000, **404**:42-49.
- Yarbro JW: **Mechanism of action of hydroxyurea.** *Semin Oncol* 1992, **19** (3 Suppl9):1-10.
- Kishony R, Leibler S: **Environmental stresses can alleviate the average deleterious effect of mutations.** *J Biol* 2003, **2**:14.
- Parsons AB, Brost RL, Ding H, Li Z, Zhang C, Sheikh B, Brown GW, Kane PM, Hughes TR, Boone C: **Integration of chemical-genetic and genetic interaction data links bioactive compounds to cellular target pathways.** *Nat Biotechnol* 2004, **22**:62-69.
- Koning AJ, Larson LL, Cadera EJ, Parrish ML, Wright RL: **Mutations that affect vacuole biogenesis inhibit proliferation of the endoplasmic reticulum in *Saccharomyces cerevisiae*.** *Genetics* 2002, **160**:1335-1352.
- Bennett CB, Lewis LK, Karthikeyan G, Lobachev KS, Jin YH, Sterling JF, Snipe JR, Resnick MA: **Genes required for ionizing radiation resistance in yeast.** *Nat Genet* 2001, **29**:426-434.
- Chang M, Bellaoui M, Boone C, Brown GW: **A genome-wide screen for methyl methanesulfonate-sensitive mutants reveals genes required for S phase progression in the presence of DNA damage.** *Proc Natl Acad Sci USA* 2002, **99**:16934-16939.
- Winzler EA, Shoemaker DD, Astromoff A, Liang H, Anderson K, Andre B, Bangham R, Benito R, Boeke JD, Bussey H, et al.: **Functional characterization of the *S. cerevisiae* genome by gene deletion and parallel analysis.** *Science* 1999, **285**:901-906.
- Elledge SJ, Davis RW: **Two genes differentially regulated in the cell cycle and by DNA-damaging agents encode alternative regulatory subunits of ribonucleotide reductase.** *Genes Dev* 1990, **4**:740-751.
- Domkin V, Thelander L, Chabes A: **Yeast DNA damage-inducible Rnr3 has a very low catalytic activity strongly stimulated after the formation of a cross-talking Rnr1/Rnr3 complex.** *J Biol Chem* 2002, **277**:18574-18578.
- Zhao X, Rothstein R: **The Dun1 checkpoint kinase phosphorylates and regulates the ribonucleotide reductase inhibitor Sml1.** *Proc Natl Acad Sci USA* 2002, **99**:3746-3751.
- Symington LS: **Role of RAD52 epistasis group genes in homologous recombination and double-strand break repair.** *Micro-*

- biol Mol Biol Rev* 2002, **66**:630-670.
38. Klein HL: **RDH54, a RAD54 homologue in *Saccharomyces cerevisiae*, is required for mitotic diploid-specific recombination and repair and for meiosis.** *Genetics* 1997, **147**:1533-1543.
 39. van den Bosch M, Zonneveld JB, Lohman PH, Pastink A: **Isolation and characterization of the RAD59 homologue of *Kluyveromyces lactis*.** *Curr Genet* 2001, **39**:305-310.
 40. Wenthe SR, Gasser SM, Caplan AJ: **Biogenesis and Function of the Yeast Vacuole.** In: *The Molecular and Cellular Biology of the Yeast Saccharomyces Volume 3*. Edited by: Pringle JR, Broach JR, Jones EW. New York: Cold Spring Harbor Laboratory Press; 1997:363-470.
 41. **Yeast Deletion Web Pages** [http://www.sequence.stanford.edu/group/yeast_deletion_project/deletions3.html]
 42. Olson MV: **When less is more: gene loss as an engine of evolutionary change.** *Am J Hum Genet* 1999, **64**:18-23.
 43. Zeyl C, Vanderford T, Carter M: **An evolutionary advantage of haploidy in large yeast populations.** *Science* 2003, **299**:555-558.
 44. Kaufer NF, Fried HM, Schwindinger WF, Jasin M, Warner JR: **Cycloheximide resistance in yeast: the gene and its protein.** *Nucleic Acids Res* 1983, **11**:3123-3135.
 45. Eisen MB, Spellman PT, Brown PO, Botstein D: **Cluster analysis and display of genome-wide expression patterns.** *Proc Natl Acad Sci USA* 1998, **95**:14863-14868.
 46. Pringle JR, Broach JR, Jones EW, Eds: *The Molecular and Cellular Biology of the Yeast Saccharomyces* New York: Cold Spring Harbor Laboratory Press; 1997.
 47. **Saccharomyces Genome Database** [<http://www.yeastgenome.org>]
 48. **Bioknowledge Library** [<http://www.incyte.com/bioknowledge>]
 49. Prado F, Cortes-Ledesma F, Huertas P, Aguilera A: **Mitotic recombination in *Saccharomyces cerevisiae*.** *Curr Genet* 2003, **42**:185-198.
 50. van den Bosch M, Lohman PH, Pastink A: **DNA double-strand break repair by homologous recombination.** *Biol Chem* 2002, **383**:873-892.
 51. Lundin C, Erixon K, Arnaudeau C, Schultz N, Jenssen D, Meuth M, Helleday T: **Different roles for nonhomologous end joining and homologous recombination following replication arrest in mammalian cells.** *Mol Cell Biol* 2002, **22**:5869-5878.
 52. Fabre F, Chan A, Heyer WD, Gangloff S: **Alternate pathways involving Sgs1/Top3, Mus81/Mms4, and Srs2 prevent formation of toxic recombination intermediates from single-stranded gaps created by DNA replication.** *Proc Natl Acad Sci USA* 2002, **99**:16887-16892.
 53. Zhao X, Muller EG, Rothstein R: **A suppressor of two essential checkpoint genes identifies a novel protein that negatively affects dNTP pools.** *Mol Cell* 1998, **2**:329-340.
 54. Liao X, Butow RA: **RTGI and RTG2: two yeast genes required for a novel path of communication from mitochondria to the nucleus.** *Cell* 1993, **72**:61-71.
 55. Liu Z, Butow RA: **A transcriptional switch in the expression of yeast tricarboxylic acid cycle genes in response to a reduction or loss of respiratory function.** *Mol Cell Biol* 1999, **19**:6720-6728.
 56. Liu Z, Sekito T, Spirek M, Thornton J, Butow RA: **Retrograde signaling is regulated by the dynamic interaction between Rtg2p and Mks1p.** *Mol Cell* 2003, **12**:401-411.
 57. Menendez J, Gancedo C: **Regulatory regions in the promoters of the *Saccharomyces cerevisiae* PYC1 and PYC2 genes encoding isoenzymes of pyruvate carboxylase.** *FEMS Microbiol Lett* 1998, **164**:345-352.
 58. Roberg KJ, Bickel S, Rowley N, Kaiser CA: **Control of amino acid permease sorting in the late secretory pathway of *Saccharomyces cerevisiae* by SEC13, LST4, LST7 and LST8.** *Genetics* 1997, **147**:1569-1584.
 59. Liu Z, Sekito T, Epstein CB, Butow RA: **RTG-dependent mitochondria to nucleus signaling is negatively regulated by the seven WD-repeat protein Lst8p.** *EMBO J* 2001, **20**:7209-7219.
 60. Almaas E, Kovacs B, Vicsek T, Oltvai ZN, Barabasi AL: **Global organization of metabolic fluxes in the bacterium *Escherichia coli*.** *Nature* 2004, **427**:839-843.
 61. Kaiser CA, Gimeno RE, Shaywitz DA: **Protein secretion, membrane biogenesis, and endocytosis.** In: *The Molecular and Cellular Biology of the Yeast Saccharomyces Volume 3*. Edited by: Pringle JR, Broach JR, Jones EW. New York: Cold Spring Harbor Laboratory Press; 1997:91-227.
 62. Raymond CK, Howald-Stevenson I, Vater CA, Stevens TH: **Morphological classification of the yeast vacuolar protein sorting mutants: evidence for a prevacuolar compartment in class E vps mutants.** *Mol Biol Cell* 1992, **3**:1389-1402.
 63. Geissler S, Siegers K, Schiebel E: **A novel protein complex promoting formation of functional alpha- and gamma-tubulin.** *EMBO J* 1998, **17**:952-966.
 64. Siegers K, Waldmann T, Leroux MR, Grein K, Shevchenko A, Schiebel E, Hartl FU: **Compartmentation of protein folding in vivo: sequestration of non-native polypeptide by the chaperonin-GimC system.** *EMBO J* 1999, **18**:75-84.
 65. Smith V, Chou KN, Lashkari D, Botstein D, Brown PO: **Functional analysis of the genes of yeast chromosome V by genetic footprinting.** *Science* 1996, **274**:2069-2074.
 66. Ross-Macdonald P, Coelho PS, Roemer T, Agarwal S, Kumar A, Jansen R, Cheung KH, Sheehan A, Symoniatis D, Umansky L, et al.: **Large-scale analysis of the yeast genome by transposon tagging and gene disruption.** *Nature* 1999, **402**:413-418.
 67. Steinmetz LM, Davis RW: **Maximizing the potential of functional genomics.** *Nat Rev Genet* 2004, **5**:190-201.
 68. Bader GD, Heilbut A, Andrews B, Tyers M, Hughes T, Boone C: **Functional genomics and proteomics: charting a multidimensional map of the yeast cell.** *Trends Cell Biol* 2003, **13**:344-356.
 69. Remold SK, Lenski RE: **Pervasive joint influence of epistasis and plasticity on mutational effects in *Escherichia coli*.** *Nat Genet* 2004, **36**:423-426.
 70. Hartwell LH, Szankasi P, Roberts CJ, Murray AW, Friend SH: **Integrating genetic approaches into the discovery of anticancer drugs.** *Science* 1997, **278**:1064-1068.
 71. Huang PH, Chiang HL: **Identification of novel vesicles in the cytosol to vacuole protein degradation pathway.** *J Cell Biol* 1997, **136**:803-810.
 72. Woudstra EC, Gilbert C, Fellows J, Jansen L, Brouwer J, Erdjument-Bromage H, Tempst P, Svejstrup JQ: **A Rad26-Def1 complex coordinates repair and RNA pol II proteolysis in response to DNA damage.** *Nature* 2002, **415**:929-933.
 73. Regelmann J, Schule T, Josupeit FS, Horak J, Rose M, Entian KD, Thumm M, Wolf DH: **Catabolite degradation of fructose-1,6-bisphosphatase in the yeast *Saccharomyces cerevisiae*: a genome-wide screen identifies eight novel GID genes and indicates the existence of two degradation pathways.** *Mol Biol Cell* 2003, **14**:1652-1663.
 74. Shieh HL, Chen Y, Brown CR, Chiang HL: **Biochemical analysis of fructose-1,6-bisphosphatase import into vacuole import and degradation vesicles reveals a role for UBC1 in vesicle biogenesis.** *J Biol Chem* 2001, **276**:10398-10406.
 75. Edwards JS, Ibarra RU, Palsson BO: **In silico predictions of *Escherichia coli* metabolic capabilities are consistent with experimental data.** *Nat Biotechnol* 2001, **19**:125-130.
 76. Csete ME, Doyle JC: **Reverse engineering of biological complexity.** *Science* 2002, **295**:1664-1669.
 77. Aitchison JD, Galitski T: **Inventories to insights.** *J Cell Biol* 2003, **161**:465-469.
 78. Burke D, Dawson D, Stearns T: *Methods in Yeast Genetics* New York: Cold Spring Harbor Laboratory Press; 2000.
 79. **Molmine** [<http://www.molmine.com>]